

Research Article

Advances in Surface Plasmon Resonance-Based Biosensor Technologies for Cancer Cell Detection

Bhishma Karki ^{1,2}, **Arun Uniyal**,³ **Amrindra Pal**,³ and **Vivek Srivastava**⁴

¹Department of Physics, Tri-Chandra Multiple Campus, Tribhuvan University, Kathmandu 44600, Nepal

²National Research Council Nepal, New Baneshwor-10, Kathmandu 44600, Nepal

³Department of ECE, DIT University, Dehradun 248009, India

⁴Department of Mechanical Engineering, ABES Engineering College, Ghaziabad, UP 201009, India

Correspondence should be addressed to Bhishma Karki; magnum.photon@gmail.com

Received 21 May 2022; Revised 16 July 2022; Accepted 25 July 2022; Published 9 September 2022

Academic Editor: Yuan-Fong Chou Chau

Copyright © 2022 Bhishma Karki et al. This is an open access article distributed under the Creative Commons Attribution License, which permits unrestricted use, distribution, and reproduction in any medium, provided the original work is properly cited.

Efforts have been made to enhance the surface sensitivity of the conventional surface plasmon resonance biosensor. To improve the sensitivity, a unique two-dimensional heterostructure layer of titanium disilicide and black phosphorus layer has been deposited over the metal surface. The titanium disilicide (TiSi₂) nanosheet is placed in between silver (Ag) and black phosphorus (BP) films in the Kretschmann arrangement. This biosensor executes better over a wide range of refractive index variations, including biological cell distribution in individual blood. It may become a fast method of detecting cancerous cells and the several variants of corona and other viruses that become pandemic. Using the finite element method-based simulation technique, the sensitivity obtained as 195.4 degree/RIU, 167.6 degree/RIU, 212.4 degree/RIU, 168.4 degree/RIU, 212.4 degree/RIU, 186.6 degree/RIU, 218.6 degree/RIU, 195.4 degree/RIU, 203.6 degree/RIU, 202.6 degree/RIU, 203.6 degree/RIU, and 202.6 for basal (skin cancer), basal (normal cell), HeLa (cervical cancer), MCF-7 (breast cancer), HeLa (normal cell), Jurkat (blood cancer), Jurkat (normal cell), PCI-2 (adrenal gland cancer), PCI-2 (normal cell), MDA-MB-231 (breast cancer), MDA-MB-231 (normal cell), MCF-7 (breast cancer), and MCF-7 (normal cell), respectively, and other performance parameters such as detection accuracy, figure of merit, and full width and half maximum (FWHM) are also evaluated.

1. Introduction

Surface plasmon resonance (SPR) has been proved effective in optical technology to accurately measure the dimension of cells or viruses that cause the deadliest cancer. SPR sensors can be used to achieve greater sensitivity and rapid detection for medical diagnostics [1]. In the present theoretical study, the Kretschmann arrangement based on angular interrogation has been used. The sensitivity is the key parameter, and it should be high. The sensitivity of conventional biosensors can be enhanced by adding the two-dimensional (2D) material to the conventional sensor [2].

Plasmonic materials such as metals are used in the SPR sensor. The most common metals, gold (Au) and silver (Ag), have been used for SPR sensor design. The oxidation of the metals and surface corrosion weakens the plasmonic

properties. However, Au is costly though having better stability and superior optical performance. Au is considered a suitable material since it is corrosion-free; however, it gives a broad resonance peak that reduces the accuracy of analyte detection. Conversely, the SPR sensor based on Ag film shows the highest resolution. Using Ag in SPR sensors, better sensitivity can be achieved, but the chemical stability is poor as it creates brittle oxide with the aqueous sensing medium [1, 3].

When we introduced a layer of 2D material, the performance of the biosensor improved. A layer of titanium disilicide is used in the proposed biosensor. The titanium disilicide (TiSi₂) is an orthorhombic transition metal having a heterostructure. However, it is a stable material that is easily oxidized when exposed to the aqueous solution. It has high absorption efficiency and provides a direct bandgap of

TABLE 1: Refractive index (RI) values for healthy and cancer cells [6].

Cancer cell	Concentration level (%)	RI
Basal (skin cancer)	0.8	1.38
Basal (normal cell)	0.3–0.7	1.36
HeLa (cervical cancer)	0.8	1.392
HeLa (normal cell)	0.3–0.7	1.368
Jurkat (blood cancer)	0.8	1.39
Jurkat (normal cell)	0.3–0.7	1.376
PCI-2 (adrenal gland cancer)	0.8	1.395
PCI-2 (normal cell)	0.3–0.7	1.381
MDA-MB-231 (breast cancer)	0.8	1.399
MDA-MB-231 (normal cell)	0.3–0.7	1.385
MCF-7 (breast cancer)	0.8	1.401
MCF-7 (normal cell)	0.3–0.7	1.387

0.5 eV at room temperature. Therefore, it has low resistivity properties and is suitable for designing biosensors [4].

Graphite is a carbon atom bonded with three neighboring atoms, while black phosphorus (BP) atoms are bounded in-plane to form 2D layers and interact through Vanderwall forces. Furthermore, the phosphorus atom has five valency shell electrons available for bonding (the valency shell configuration is $3p^23p^3$). Each phosphorus atom has a lone pair of highly reactive electrons to air. Thus, the property of BP enhances the sensitivity of the proposed structure [5].

Cancer is a disease in which somebody's cells grow uncontrollably and spread to other body parts. The human body is made up of trillions of cells; these cells grow and multiply, called cell division. When cells grow old, they die naturally. The new cells take over. Breaking down the orderly process, abnormal cells grow and then multiply to form tumors, the lump of tissue. The tumors may be cancerous or may not but can travel to different body parts to form new tumors. More than a hundred types of cancer are illustrated elsewhere and usually named for the host organ, such as lung cancer and brain cancer. There are specific types of cells; the first is carcinoma, the most common type of cancer. The second is adeno carcinomas, which form epithelial cells that produce fluids or mucus. Most cancers of the breast, colon, and prostate are adeno carcinoma. Basal cell carcinoma is cancer that begins in the base layer of the epidermis. Among different types of cancer, Jurkat (blood cancer), HeLa (cervical cancer), PCI-2 (adrenal gland cancer), (MDA-MB-231 breast cancer type-1), MCF-7 (breast cancer type-2), and basal (skin cancer) are the most dominating [6]. The dimensions of these cells are in nanometres, which is not easily measurable. Therefore, the refractive index parameter measures the patient's blood sample. The refractive index values are given in Table 1 for selected cancer types [7–17].

Prism-based SPR sensors and PCF-based sensors have been reported earlier by many researchers. Ahmed et al. [18] proposed a photonic crystal fiber (PCF) based optical sensor for sensing various blood components. At $f=1.5$ THz, a relatively higher sensitivity response was achieved for red blood cells (RBCs) (80.93%), for hemoglobin, white blood cells (WBCs), plasma, and water, it was 80.56%, 80.13%,

79.91%, and 79.39%, respectively. Besides this, Jabin et al. [19] proposed a dual-core PCF-based SPR biosensor for detecting various human blood samples. The performance parameters like wavelength selectivity, resolution, amplitude sensitivity, FoM with detection limit, and transmittance variance have been calculated. Some other research fellows also proposed PCF-based optical sensors for applications like alcohol sensing [20], gas sensing [21], and plasma detection [22]. Many other plasmonic structures like plasmonic absorber (with two bands) and refractive index sensors based on metal insulator metal (MIM) waveguide were proposed by [23–27].

The proposed method can identify cancer cells in real time, which is impossible with current techniques. Cancer screening: diagnosing cancer at its earliest stages often provides the best cure. Studies show that screening tests can save lives by diagnosing cancer early. Other cancer screening tests are recommended why for people with increased risk.

A laboratory test, such as a urine and blood test, may identify abnormalities caused due to cancer. The complete blood count may reveal an unusual number or type of white blood cells. There are several imaging tests such as computerized tomography (CT) scan, magnetic resonance imaging (MRI) scan, positron emission tomography (PET) scan, ultrasound and X-ray, and cancer sample tests in a laboratory.

Normal cells look uniform, with similar sizes and orderly organization. Cancer cells look less orderly, with varying sizes and different organizations. An antibody test is another blood test preferred as a possible diagnostic tool. The immune system makes antibodies to help fight off foreign invaders like bacteria and viruses in the human body. The immune system also makes antibodies in response to cancer cells. The antibody test is not full proof and needs further improvement. Genetic blood tools: with a strong family history of cancer, a tumor marker test detects a higher protein in blood when cancer is present. The protein can be high in both ovarian and breast cancer. In conclusion, blood tests may eventually have a role in early cancer detection or its recurrences.

2. Theoretical Modeling for the Proposed Sensor

Figure 1 shows the layered structure in the Kretschmann arrangement on $TiSi_2$. The monochromatic light (633 nm) is incident on the BK7 prism. Refracted to the different layers comes out in the opposite direction with changing features following the rules of total internal reflection (TIR). The prism is covered with the thin layer of Ag of coating $D_1 = 45$ nm; this Ag film is then covered by two-dimensional (2D) $TiSi_2$ nanolayer's $D_2 = P * 2$ nm (where P is the number of $TiSi_2$ films), which in turn is covered with a BP thin film of coating $D_3 = B * 0.5$ nm (where B is the number of BP films). BP layer is interpolated between $TiSi_2$ film and sensing medium. The role of the BP film is to enhance the bimolecular recognition element. The BK7 prism is used as a coupling prism. The design parameters of the proposed sensor are given in Table 2. Table 2 indicates the design

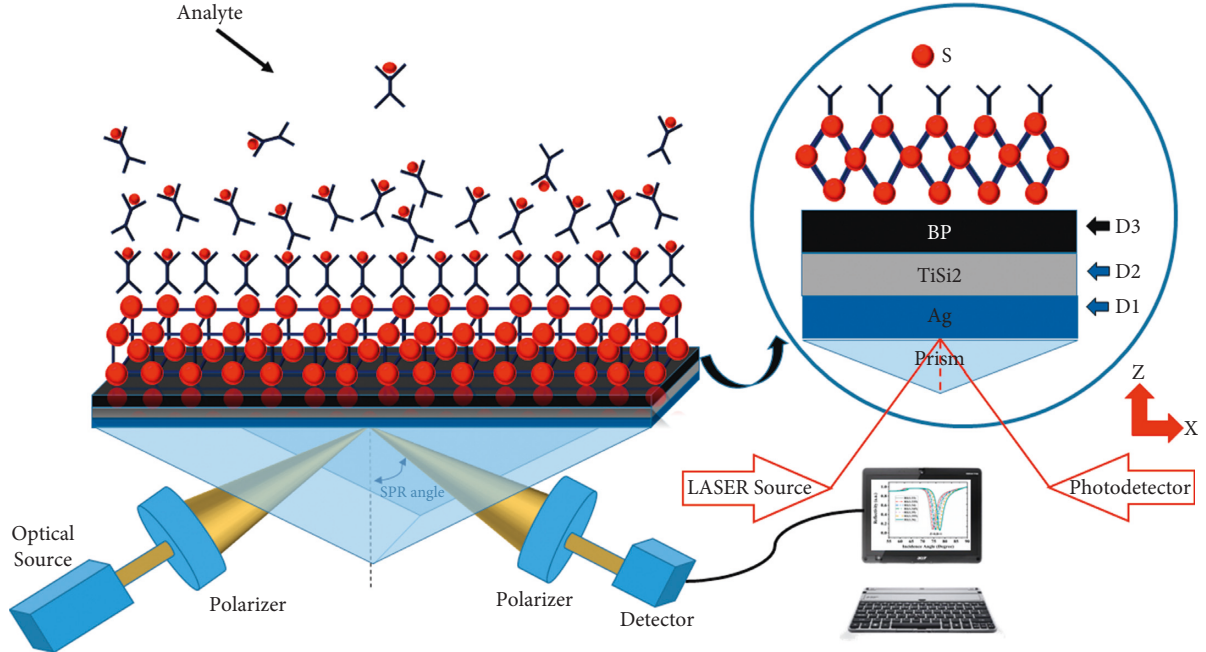


FIGURE 1: The schematic diagram for the proposed sensor.

TABLE 2: Design parameter for the proposed SPR biosensor.

Material used	RI of the material at 633 nm		Thickness (nm)	References
	Real part (n)	Imaginary part (k)		
Prism BK7	1.515			[29]
Ag, metal	0.056253	4.2760	$D_1 = 45$	[30]
TiSi ₂	2.70008	2.939449	$D_2 = P * 2$	[4]
BP	3.531	0.04087	$D_3 = B * 0.5$	[5]

parameters like a layer of the material, refractive index (RI), coating thickness, and material used for the proposed work. The BK7 prism is used as a coupling prism; the refractive index (RI) of the prism is given as [28]

$$n_{pBK7} = \left(\frac{\alpha_1 \lambda^2}{\lambda^2 - \beta_1} + \frac{\alpha_2 \lambda^2}{\lambda^2 - \beta_2} + \frac{\alpha_3 \lambda^2}{\lambda^2 - \beta_3} + 1 \right)^{1/2}, \quad (1)$$

where λ is the wavelength (nm) of the used optical signal. The values of the constants α_1 , α_2 , α_3 , β_1 , β_2 , and β_3 are 1.03961212, 0.231792344, 1.01046945, 0.00600069867, 0.0200179144, and 103.560653, respectively. The RI of the thin metal layer (Ag) is mathematically expressed using Drude's model [36], $n_{Ag} = (1 - \lambda^2 * \lambda_c / \lambda_p^2 (\lambda_c + \lambda * i))^{1/2}$, where $\lambda_c = 17.614 \mu\text{m}$ and $\lambda_p = 0.14541 \mu\text{m}$. The RI of TiSi₂ (n_{TiSi_2}) at 2 nm thickness is $2.70008 + i * 0.939449$ in the visible range. The RI of BP is given as $n_{BP} = 3.531 - i * 0.04087$.

The sensing performance of the systems is evaluated by the transfer matrix method [37].

The formula estimates the reflectance

$$r_{pm_1d_1m_2d_2} = \frac{r_{pm_1} + r_{m_1d_1m_2d_2} e^{2iK_{m_1x}d_{m_1}}}{1 + r_{pm_1d_1m_2d_2} e^{2iK_{m_1x}d_{m_1}}}, \quad (2)$$

where

$$K_{ix} = \left(\left(\frac{2\pi}{\lambda} \right)^2 \epsilon_i - K_z^2 \right)^{1/2}, \quad i = p, m_1, d_1, m_2, d_2,$$

$$r_{pm} = \frac{(\epsilon_m K_{px} - \epsilon_p K_{mx})}{(\epsilon_m K_{px} + \epsilon_p K_{mx})}, \quad (3)$$

$$r_{md} = \frac{(\epsilon_d K_{mx} - \epsilon_d K_{dx})}{(\epsilon_d K_{mx} + \epsilon_m K_{dx})},$$

p , m , and d indicate the prism, metal, and dielectric, respectively. The dip in the resonance curve can be written as

$$K_{sp} = \frac{2\pi}{\lambda} n_s \sin \theta_{SPR} = \text{Real} \left(\frac{2\pi}{\lambda} \sqrt{\frac{\epsilon_m \epsilon_s}{\epsilon_m + \epsilon_s}} \right), \quad (4)$$

n_0 is the RI of the sensing layer, ϵ_s and ϵ_m are the dielectric constants of the analyte and metal, respectively, angle of resonance is θ_{SPR} , and K_{sp} is the propagation constant. The reflectance is defined as $R_P = |r_{pm_1d_1m_2d_2}|^2$, where $r_{pm_1d_1m_2d_2}$ is the reflection coefficient of the incident optical signal. The sensitivity is represented as $S_n = \delta \theta_{SPR} / \delta n_s$, where $\delta \theta_{SPR}$ and δn_s are the changes in the resonance angle and the RI of the sensing layer, respectively.

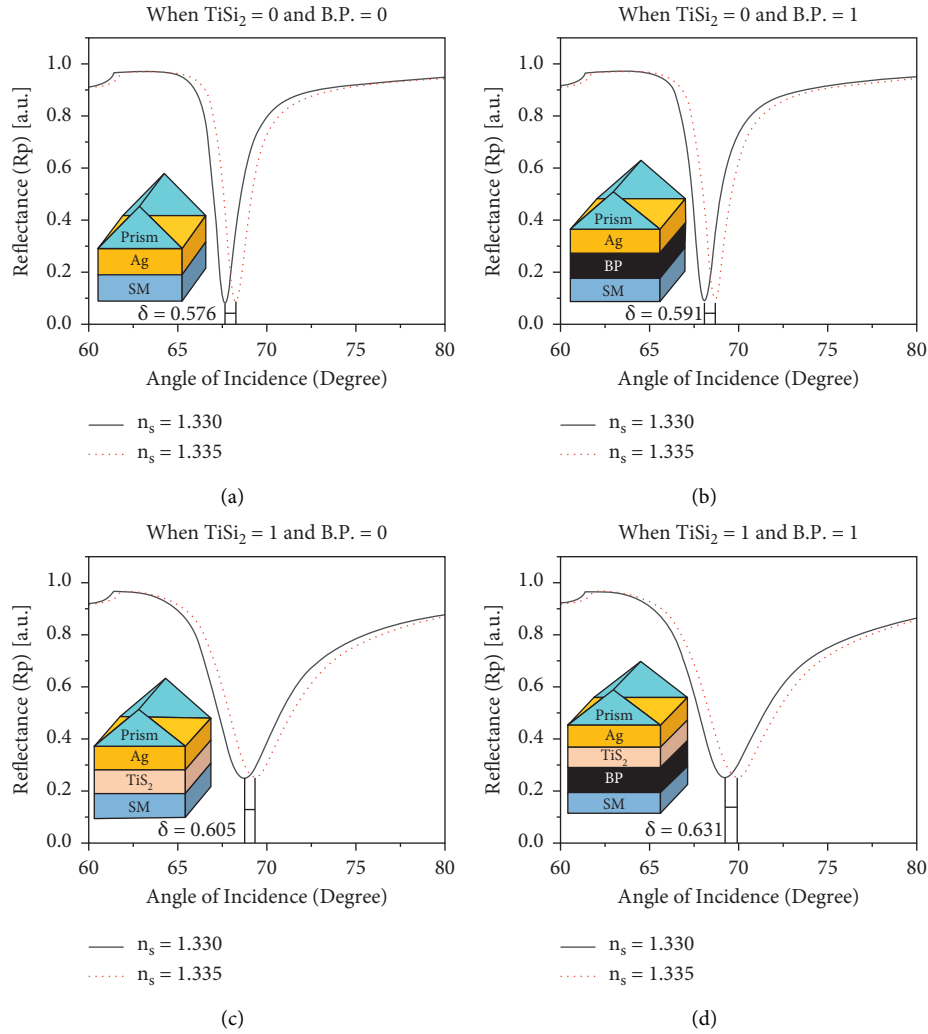


FIGURE 2: The SPR curves for change in $TiSi_2$ and BP layers. (a) $P=0, B=0$. (b) $P=0, B=1$. (c) $P=1, B=0$. (d) $P=1, B=1$, the same RI change.

Table 2 indicates the design parameters like a layer of the material, refractive index (RI), coating thickness, and material used for the proposed work. The whole study has done with the help of the MATLAB simulation tool, and the results are verified using COMSOL Multiphysics 5.6 version.

3. Results and Discussion

The sensitivity and detection accuracy are the performance parameters of the biosensor [38], and the same is computed for the proposed biosensor. The sensitivity of the biosensor is represented as $S = \delta\theta_{SPR}/\delta n$, where δn is the change in the RI. The biosensor's detection accuracy (DA) can be expressed as $DA = 1/FWHM$, where FWHM is the width of the spectra of the SPR curve; at that point, the reflectivity is 50% of the maximum value. The high value of the sensitivity and DA is desirable [31]. The figure of merit can be expressed as $FoM = S \cdot DA = S/FWHM$ [32]. It directly depends on the FWHM and sensitivity. The sensitivity characteristics of the modified Kretschmann structure are investigated here by adding $TiSi_2$ nanosheet and BP. To show the enhancement of

the sensitivity performance, the variation in the reflectance of the biosensor as a function of the incident angle at the various refractive indices of the sensing layer is shown in Figure 2. In Figure 2(a), the number of layers in the structure is ($TiSi_2 = 0$ and $BP = 0$), which means $TiSi_2$ and BP layers are not present in the biosensor (conventional sensor). The sharp downfall in the reflectance curve is found at the range of specific angles due to the SPR excitation. This phenomenon shows that the sensor absorbs the incident light due to generated surface plasmons. However, the change in the RI of the sensing layer (contact layer) due to molecular interaction is very low. The resonance dip has a small excursion of about $\delta\theta = 0.576^\circ$ with minimum reflectance of 0.08454 and sensitivity obtained as $115.2^\circ/RIU$ for the conventional sensor. In Figure 2(b), the biosensor has only a BP layer ($TiSi_2 = 0$ and $BP = 1$), and the remaining parameter is the same. The resonance offset dip increases and is found as $\delta\theta = 0.591^\circ$ with minimum reflectance of 0.09036 and sensitivity obtained as $118.2^\circ/RIU$, which is higher than the previous case when $TiSi_2$ and BP layers are not present in the biosensor. Now, the $TiSi_2$ sheet is taken into consideration

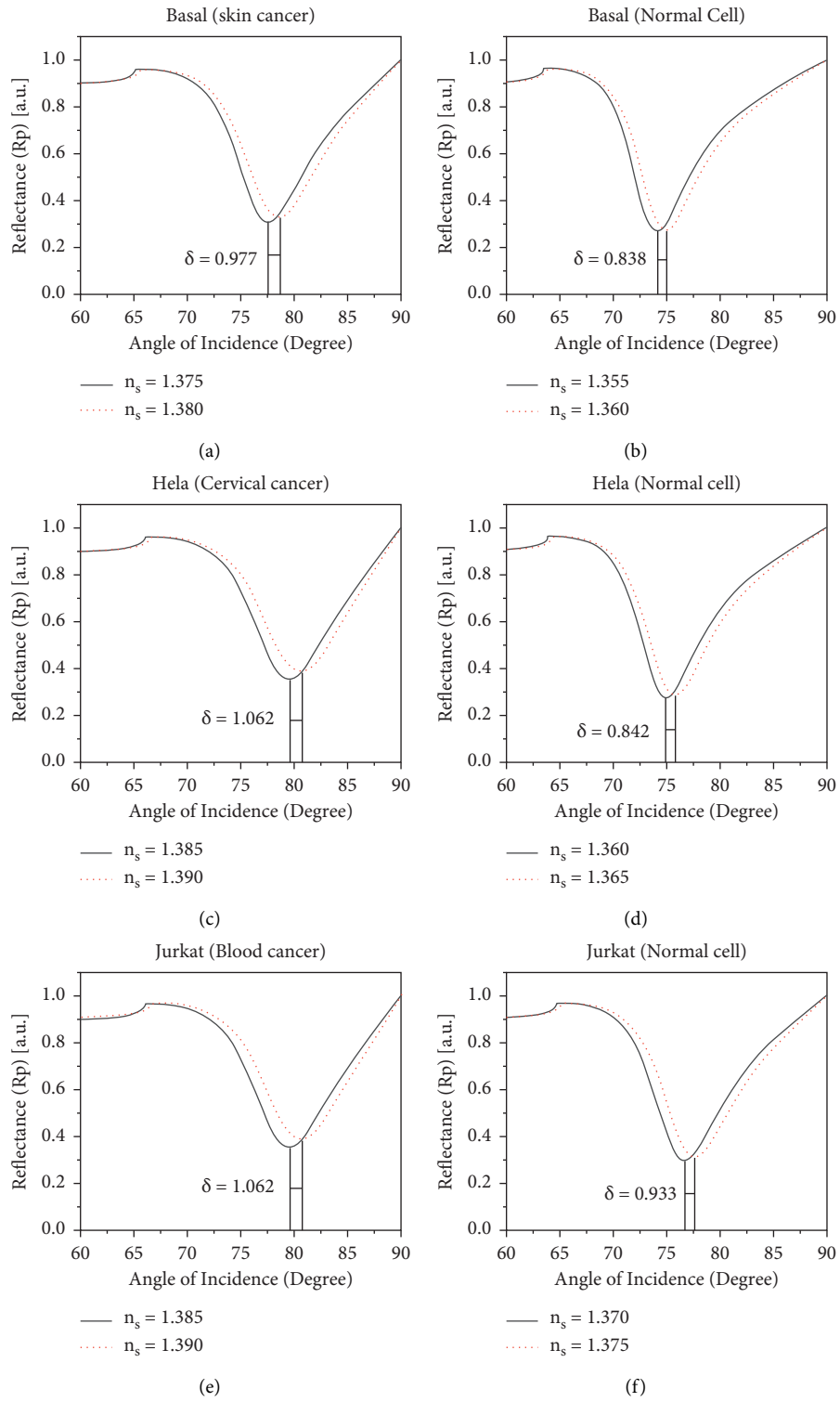


FIGURE 3: Continued.

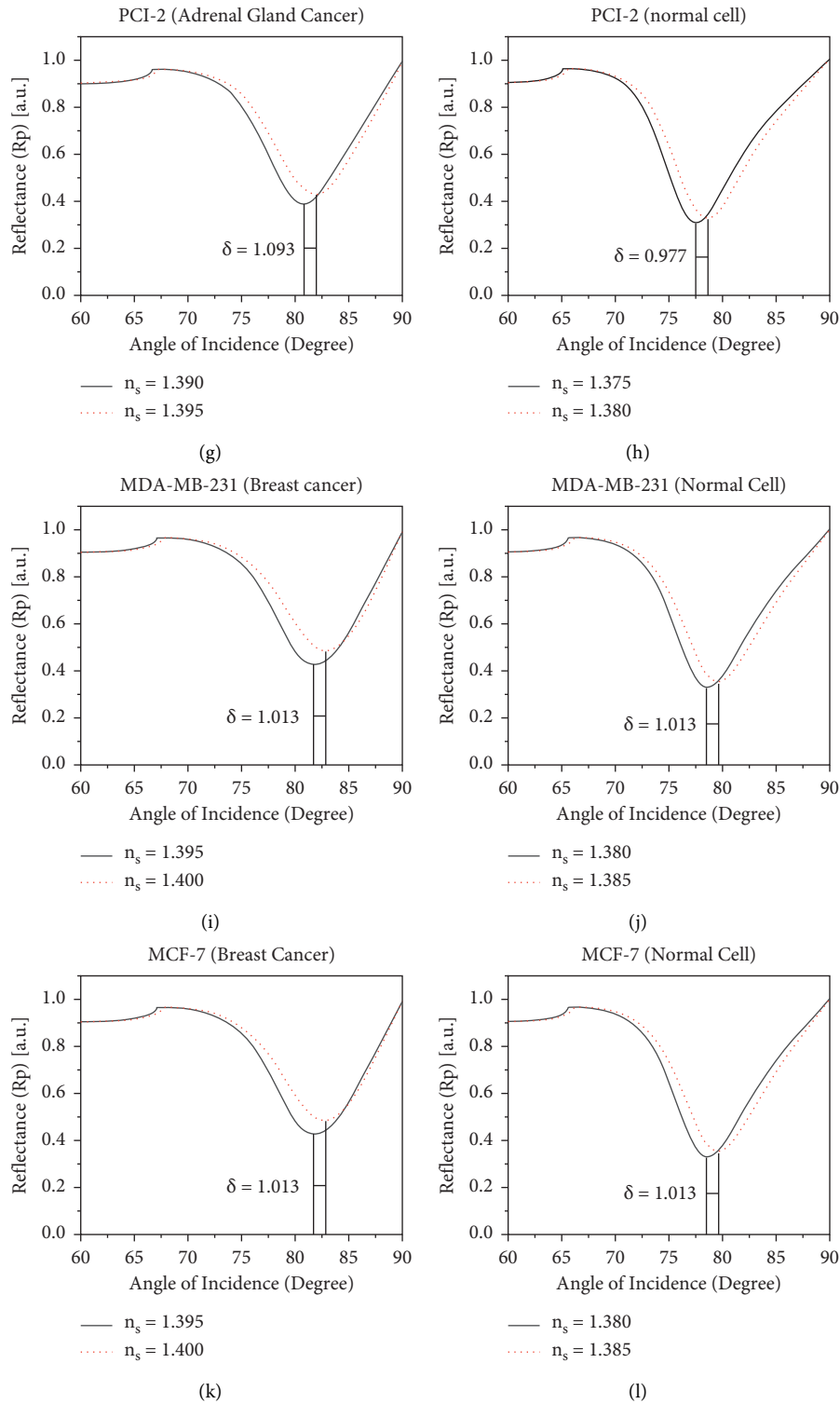


FIGURE 3: Reflectance vs. angle of incidence of targeted cancerous cells.

and ignores the BP ($TiSi_2=1$ and $BP=0$), the resonance angle is obtained as $\delta\theta = 0.605^\circ$ with minimum reflectance of 0.25395, and sensitivity is obtained as $121^\circ/RIU$ (Figure 2(c)). $TiSi_2$ and BP layers ($TiSi_2=1$ and $BP=1$) are added to the structure, and this modification greatly shifts

the dip in the resonance curve. The resonance angle is obtained as $\delta\theta = 0.631^\circ$ with minimum reflectance of 0.25363 and sensitivity is obtained as $126.2^\circ/RIU$ as shown in Figure 2(d). In the comparative study of the relevant data, it is found that the resonance angle offset is larger in the

TABLE 3: Performance parameters when layer of $\text{TiSi}_2 = 1$ and layer of BP = 3 at 633 nm wavelength.

Type of cell	RI of cell	Targeted RI	Minimum reflectance	S	θ_1	θ_2	FWHM	DA	FoM
Basal (skin cancer)	1.38	1.38	0.33046	195.4	75.26	80.6	5.38	0.19	36.32
Basal (normal cell)	1.36	1.36	0.27794	167.6	72.04	77.1	5.04	0.20	33.25
HeLa (cervical cancer)	1.392	1.39	0.38627	212.4	77.24	82.4	5.2	0.19	40.85
HeLa (normal cell)	1.368	1.365	0.28677	168.4	72.78	77.9	5.16	0.19	32.64
Jurkat (blood cancer)	1.39	1.39	0.38627	212.4	77.24	82.4	5.2	0.19	40.85
Jurkat (normal cell)	1.376	1.375	0.31213	186.6	74.38	79.7	5.35	0.19	34.88
PCI-2 (adrenal gland cancer)	1.395	1.395	0.42904	218.6	78.4	83.2	4.83	0.21	45.26
PCI-2 (normal cell)	1.381	1.38	0.33046	195.4	75.26	80.6	5.38	0.19	36.32
MDA-MB-231 (breast cancer)	1.399	1.4	0.48642	203.6	79.8	83.8	4.01	0.25	50.77
MDA-MB-231 (normal cell)	1.385	1.385	0.35444	202.6	76.2	81.6	5.36	0.19	37.80
MCF-7 (breast cancer)	1.401	1.4	0.48642	203.6	79.8	83.8	4.01	0.25	50.77
MCF-7 (normal cell)	1.387	1.385	0.35444	202.6	76.2	81.6	5.36	0.19	37.80

proposed biosensor in contrast with the conventional sensor due to the addition of TiSi_2 and BP layers. The proposed work improves the sensor's sensitivity by adding the TiSi_2 and BP layers.

To target the refractive index values of cancer types shown in Table 1, a four-layer combination has been optimized. Figure 3 depicts the reflectance vs. angle of incidence of the proposed biosensor for a different cancerous cell. Figure 3(a) depicts the SPR curve for basal (skin cancer) where 195.4 degree/RIU sensitivity has been achieved, with quality factor 36.32, detection accuracy 0.19, and FWHM 5.38. Figure 3(b) shows the SPR curve for basal (normal cell) where 167.6 degree/RIU sensitivity has been attained, quality factor is 33.25, detection accuracy is 0.20, and FWHM is 5.04. Figure 3(c) represents the SPR curve for HeLa (cervical cancer) with a difference of 0.002 of actual 1.392 and targeted 1.39 RI, 212.4 degree/RIU sensitivity has been evaluated, quality factor is 40.85, detection accuracy is 0.19, and FWHM is 5.2. Figure 3(d) depicts the SPR curve for HeLa (normal cell) with a difference of 0.003 of actual 1.368 and targeted 1.365 RI, 168.4 degree/RIU sensitivity has been calculated where quality factor is 32.64, detection accuracy is 0.19, and FWHM is 5.16. Figure 3(e) illustrates the SPR curve for Jurkat (blood cancer) where 212.4 degree/RIU sensitivity has been achieved, with a quality factor of 40.85, detection accuracy of 0.19, and FWHM of 5.2. Figure 3(f) represents the SPR curve for Jurkat (normal cell) with a difference of 0.001 of actual 1.376 and targeted 1.375 RI, 186.6 degree/RIU sensitivity has been reported where quality factor is 34.88, detection accuracy is 0.19, and FWHM is 5.35. Figure 3(g) shows the SPR curve for PCI-2 (adrenal gland cancer) where 218.6 degree/RIU sensitivity has been obtained, and quality factor is 45.26, detection accuracy is 0.21, and FWHM is 4.83. Figure 3(h) shows the SPR curve for PCI-2 (normal cell) with a difference of 0.001 of actual 1.381 and targeted 1.380 RI, 195.4 degree/RIU sensitivity has been estimated where quality factor is 36.32, detection accuracy is 0.19, and FWHM is 5.38. Figure 3(i) depicts the SPR curve for MDA-MB-231 (breast cancer) with a difference of 0.001 of actual 1.399 and targeted 1.4 R.I, 203.6 degree/RIU sensitivity has been achieved where quality factor is 50.77, detection accuracy is 0.25, and FWHM is 4.01. Figure 3(j) shows the SPR curve for MDA-MB-231

(normal cell), where 202.6 degree/RIU sensitivity has been found with a quality factor 37.80, detection accuracy 0.19, and FWHM 5.36. Figure 3(k) represents the SPR curve for MCF-7 (breast cancer) with a difference of 0.001 of actual 1.399 and targeted 1.4 RI, 203.6 degree/RIU sensitivity has been where quality factor is 50.77, detection accuracy is 0.25, and FWHM is 4.01. Figure 3(l) depicts the SPR curve for MCF-7 (normal cell) with a difference of 0.002 of actual 1.387 and targeted 1.385 RI, 202.6 degree/RIU sensitivity has been achieved where quality factor is 37.80, detection accuracy is 0.19, and FWHM is 5.36. The sensitivity and detection accuracy are the performance parameters of the biosensor, and the same is computed for the proposed biosensor.

Table 3 presents all these parameters while a layer of $\text{TiSi}_2 = 1$ and BP = 3 at 633 nm wavelength.

In Figure 4, for the better explanation of the proposed SPR biosensor, the electric field intensity plot with respect to distance from prism interface has been plotted. In Figure 4(a), Ag and TiSi_2 without the BP layer and, in Figure 4(b), Ag, TiSi_2 with the BP layer has been investigated. It is observed that when the RI of analyte varies from 1.330 to 1.335 with the BP layer, the greater enhancement in the electric field has been observed. This shows strong surface plasmon (SP) excitation. A slight change in RI of the sensing medium near the interface results in a large change in the surface wave characteristic which in turn causes the change in electric field.

4. Structure Parameters Optimization

Effects of the thickness of the metal layer and the number of TiSi_2 and BP layers on the reflectance of the SPR sensor have been investigated in this section. As illustrated in Figure 5(a), different Ag layer thicknesses between 35 and 50 nm are employed. The calculated and determined values of minimum reflectance are 0.10667, 0.25538, 0.01405, and 0.41888 for an Ag layer thickness of 35 nm, 40 nm, 45 nm, and 50 nm, respectively. So, the optimized thickness of the Ag layer of 45 nm is considered. Next, the thickness of a TiSi_2 sheet is 2 nm. For the thickness of TiSi_2 taken as 2 nm, 3 nm, and 4 nm, the values of minimum reflectance were computed as 0.25538, 0.3951, and 0.4979, respectively. The SPR dip is not

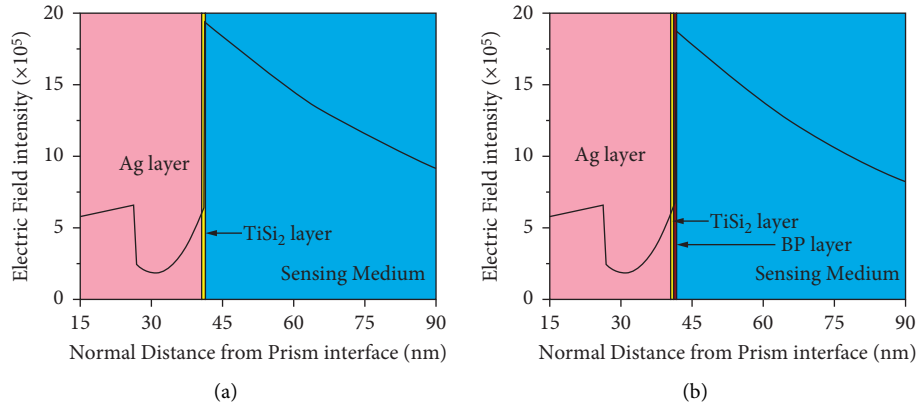


FIGURE 4: Electric field intensity plot (a) without BP layer and (b) with BP layer.

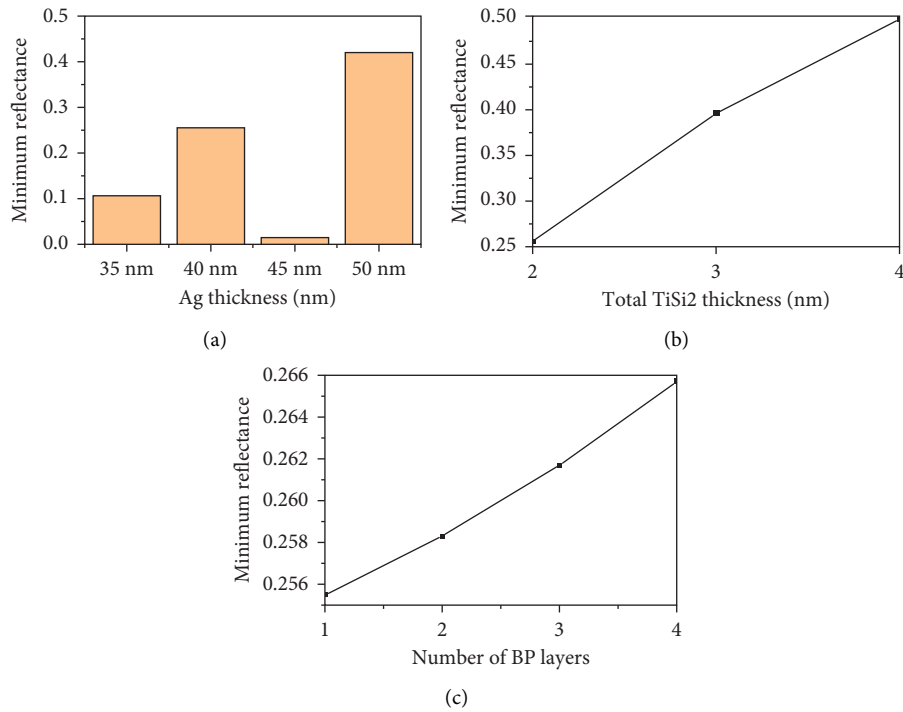


FIGURE 5: Minimum reflectance variations by varying the (a) Ag layer thickness, (b) TiSi₂ layer thickness, and (c) the number of BP layers.

TABLE 4: Comparison of the present work with earlier reported works.

Reference	Layers with prism	S (degree/RIU)	FWHM (degree)	DA (degree ⁻¹)	FoM (RIU ⁻¹)
[28]	Ag-SnSe-BlueP-MOS ₂	187		0.35	24.60
[33]	Au-BP-Au-graphene	218	8.34	—	26.13
[32]	Au-WSe ₂	179.32		0.17	—
[34]	TiO ₂ -Ag-MoSe ₂ -graphene	194	—	0.2702	54.04
Present work	Ag-TiSi ₂ -BP	218.6	4.83	0.21	45.26

obtained for more than 4 nm thickness of TiSi₂. So, the optimum thickness of TiSi₂ sheet is 2 nm (Figure 5(b)). A monolayer of BP is taken in this case. In the similar manner, the number of BP layers altered from 1 to 4 and the values of minimum reflectance are computed. The computed values

for minimum reflectance are 0.2555, 0.2583, 0.2617, and 0.2657 for a number of BP layers as 1, 2, 3, and 4, respectively, shown in Figure 5(c).

So, the optimized value for the BP layer is considered as 0.5 nm. A monolayer of TiSi₂ is taken in this case.

At last, a comparative table (Table 4) shows the proposed biosensor's computed parameters with the previously reported works.

5. Conclusion

To identify cancer cells, several approved techniques include the blood culture, urine test, stool test, and biopsy. A prolonged period maybe two years because the cancer cells are changing their dimension, and the tumors are moving from point to point. To zero in to declare cancer and its type, we lose precious time, and suitable medication or radiation therapy begins when survival chances are less. Following the principle of surface plasmon resonance, the proposed optical method is useful for detecting cancer at an early stage. The proposed method has been optimized to cater to five different cancer cells having a refractive index, namely, basal skin cancer (RI-1.38), basal normal cell (RI-1.36), Jurkat blood cancer (RI-1.39), PCI-2 adrenal gland cancer (RI-1.395), and MDA-MB-231 normal cell (RI-1.385) as it is based on the principle to investigate the refractive index of the blood sample of the patient. Furthermore, we plan to optimize the combination of metal 2D material with finite dimensions to cater to more cancer cells and make the device highly economical [35].

Data Availability

No data available on request.

Conflicts of Interest

The authors declare that they have no conflicts of interest.

References

- [1] S. Natarajan, B. Karki, K. P. Rane, A. Jha, and A. Pal, "Tuning and sensitivity improvement of bi-metallic structure-based surface plasmon resonance biosensor with 2-d ϵ -tin selenide nanosheets," *Plasmonics*, vol. 17, 2022.
- [2] M. G. Daher, S. A. Taya, S. K. Patel, M. M. Olaimat, and O. Ramahi, "Surface plasmon resonance biosensor based on graphene layer for the detection of waterborne bacteria," *Journal of Biophotonics*, vol. 15, no. 5, Article ID e202200001, 2022.
- [3] A. Jha and A. Jha, "A theoretical analysis on sensitivity improvement of an spr refractive index sensor with graphene and barium titanate nanosheets," *Optik*, vol. 231, Article ID 166378, 2021.
- [4] V. R. Balaji, "A theoretical analysis to improve the tuning and sensitivity of a surface plasmon resonance biosensor employing titanium disilicide-graphene heterostructures," *Journal of Computational Electronics*, vol. 21, no. 1, pp. 263–269, 2022.
- [5] Y. Singh and S. K. Raghuvanshi, "Sensitivity enhancement of the surface plasmon resonance gas sensor with black phosphorus," *IEEE Sensors Letters*, vol. 3, no. 12, 2019.
- [6] M. G. Daher, S. A. Taya, D. Vigneswaran et al., "Design of a nano-sensor for cancer cell detection based on a ternary photonic crystal with high sensitivity and low detection limit," *Chinese Journal of Physics*, vol. 77, pp. 1168–1181, 2022.
- [7] A. N. Yaroslavsky, R. Patel, E. Li, C. Lin, M. Al-Arashi, and V. Neel, "High-contrast mapping of basal cell carcinomas," *Optics Letters*, vol. 37, no. 4, pp. 644–646, 2012.
- [8] R. Hinz and B. Hinz, "Inhibition of cancer cell invasion by cannabinoids via increased expression of tissue inhibitor of matrix metalloproteinases-1," *Journal of the National Cancer Institute*, vol. 100, no. 1, pp. 59–69, 2008.
- [9] R. Cailleau, R. Young, M. Reeves, and W. J. Reeves Jr., "Breast tumor cell lines from pleural Effusions2," *Journal of the National Cancer Institute: Journal of the National Cancer Institute*, vol. 53, no. 3, pp. 661–674, 1974.
- [10] H. Chopra, R. S. Painam, and B. Painam, "Photonic crystal waveguide-based biosensor for detection of diseases," *Journal of Nanophotonics*, vol. 10, no. 3, Article ID 036011, 2016.
- [11] M. H. Sani and S. Khosroabadi, "A novel design and analysis of high-sensitivity biosensor based on nano-cavity for detection of blood component, diabetes, cancer and glucose concentration," *IEEE Sensors Journal*, vol. 20, no. 13, 2020.
- [12] L. C. Clark Jr., "Implantable gas-containing biosensor and method for measuring an analyte such as glucose," US Patent, 1988.
- [13] L. Hajba and A. Guttman, "Circulating tumor-cell detection and capture using microfluidic devices," *TRAC Trends in Analytical Chemistry*, vol. 59, 2014.
- [14] F.-R. Li, Q. Li, H.-X. Zhou, H. Deng, and C.-Y. Deng, "Detection of circulating tumor cells in breast cancer with a refined immunomagnetic nanoparticle enriched assay and nested-RT-PCR," *Nanomedicine: Nanotechnology, Biology and Medicine*, vol. 9, no. 7, pp. 1106–1113, 2013.
- [15] T. Li, Q. Fan, T. Zhu, J. Zhao, and G. Li, "Detection of breast cancer cells specially and accurately by an electrochemical method," *Biosensors and Bioelectronics*, vol. 25, no. 12, pp. 2686–2689, 2010.
- [16] T. D. Bradley, Y. Wang, M. Alharbi et al., "Optical properties of low loss (70 db/km) hypocycloid-core kagome hollow core photonic crystal fiber for rb and cs based optical applications," *Journal of Lightwave Technology*, vol. 31, no. 16, 2013.
- [17] Y. Zhao, D. Wu, and R.-Q. Lv, "Magnetic field sensor based on photonic crystal fiber taper coated with ferrofluid," *IEEE Photonics Technology Letters*, vol. 27, no. 1, pp. 26–29, 2014.
- [18] K. Ahmed, F. Ahmed, S. Paul, M. N. Aktar, D. Vigneswaran, and M. S. Islam, "Refractive index-based blood components sensing in terahertz spectrum," *IEEE Sensors Journal*, vol. 19, no. 9, pp. 3368–3375, 2019.
- [19] M. Jabin, K. Ahmed, B. K. Paul, Y. Luo, and D. Vigneswaran, "Titanium-coated dual-core d-shaped spr-based pcf for hemoglobin sensing," *Plasmonics*, vol. 14, no. 6, pp. 1601–1610, 2019.
- [20] K. Ahmed, M. J. Haque, M. A. Jabin, B. K. Paul, I. S. Amiri, and P. Yupapin, "Tetra-core surface plasmon resonance based biosensor for alcohol sensing," *Physica B: Condensed Matter*, vol. 570, 2019.
- [21] E. R. Paul, S. Asaduzzaman, M. S. Islam, K. Ahmed, I. S. Amiri, and R. Zakaria, "Design and analysis of slotted core photonic crystal fiber for gas sensing application," *Results in Physics*, vol. 11, pp. 643–650, 2018.
- [22] K. Ahmed, B. K. Paul, A. N. Z. Rashed, R. Maheswar, I. S. Amiri, and P. Yupapin, "Design of d-shaped elliptical core photonic crystal fiber for blood plasma cell sensing application," *Results in Physics*, vol. 12, pp. 2021–2025, 2019.
- [23] C.-T. C. Chao, C. C. Yuan-Fong, A. H. Mahadi, M. R. Rahimi Kooh, N. T. R. N. Kumara, and C. Hai-Pang, "Plasmonic refractive index sensor based on the combination of

- rectangular and circular resonators including baffles,” *Chinese Journal of Physics*, vol. 71, pp. 286–299, 2021.
- [24] C. C. Yuan-Fong, C. C. Chung-Ting, S. Z. B. Haji Jumat et al., “Improved refractive index-sensing performance of multi-mode fano-resonance-based metal-insulator-metal nanostructures,” *Nanomaterials*, vol. 11, no. 8, 2021.
- [25] C. C. Yuan-Fong, C. C. Chung-Ting, H. J. Huang et al., “Ultrawide bandgap and high sensitivity of a plasmonic metal-insulator-metal waveguide filter with cavity and baffles,” *Nanomaterials*, vol. 10, no. 10, 2020.
- [26] C.-T. Chou Chao, Y.-F. Chou Chau, and H.-P. Chiang, “Enhancing plasmonic effect in periodic nanometal square prisms with fences and cavities for refractive index and temperature sensing applications,” *Journal of Nanoparticle Research*, vol. 22, no. 9, 2020.
- [27] C.-T. Chou Chao, Y.-F. Chou Chau, and H.-P. Chiang, “Highly sensitive metal-insulator-metal plasmonic refractive index sensor with a centrally coupled nanoring containing defects,” *Journal of Physics D: Applied Physics*, vol. 54, no. 11, Article ID 115301, 2021.
- [28] B. Hossain, A. K. Paul, M. A. Rahman, A. K. Sarkar, and L. F. Abdulrazak, “A highly sensitive surface plasmon resonance biosensor using sncse allotrope and heterostructure of bluep/mos2 for cancerous cell detection,” *Optik*, vol. 252, Article ID 168506, 2022.
- [29] A. Uniyal, B. Chauhan, A. Singh, and Y. Singh, “Surface plasmon biosensor based on Bi₂Te₃ antimonene heterostructure for the detection of cancer cells,” *Applied Optics*, vol. 61, no. 13, pp. 3711–3719, 2022.
- [30] B. Karki, S. Sharma, Y. Pal, and A. Pal, “Sensitivity enhancement of surface plasmon resonance biosensor with 2-d franckeite nanosheets,” *Plasmonics*, vol. 17, no. 1, pp. 71–78, 2022.
- [31] B. D. Gupta and R. K. Verma, “Surface plasmon resonance-based fiber optic sensors: principle, probe designs, and some applications,” *Journal of Sensors*, vol. 200912 pages, Article ID 979761, 2009.
- [32] D. T. Nurrohman and N.-F. Chiu, “Surface plasmon resonance biosensor performance analysis on 2d material based on graphene and transition metal dichalcogenides,” *ECS Journal of Solid-State Science and Technology*, vol. 9, no. 11, Article ID 115023, 2020.
- [33] Y. Singh, M. Paswan, and S. K. Raghuvanshi, “Sensitivity enhancement of spr sensor with the black phosphorus and graphene with bi-layer of gold for chemical sensing,” *Plasmonics*, vol. 16, no. 5, pp. 1781–1790, 2021.
- [34] M. Moznuzzaman, M. R. Islam, and M. R. Islam, “Nanolayered surface plasmon resonance-based highly sensitive biosensor for virus detection: a theoretical approach to detect sars-cov-2,” *AIP Advances*, vol. 11, no. 6, Article ID 065023, 2021.
- [35] A. Uniyal, B. Chauhan, A. Pal, and V. Srivastava, “InP and graphene employed surface plasmon resonance sensor for measurement of sucrose concentration: a numerical approach,” *Optical Engineering*, vol. 61, no. 5, 2022.
- [36] B. Karki, A. Uniyal, B. Chauhan, and A. Pal, “Sensitivity enhancement of a graphene, zinc sulfide-based surface plasmon resonance biosensor with an Ag metal configuration in the visible region,” *Journal of Computational Electronics*, vol. 21, 2022.
- [37] P. S. Pandey, S. K. Raghuvanshi, and Y. Singh, “Enhancement of the sensitivity of a surface plasmon resonance sensor using a nobel structure based on barium,” *Optical and Quantum Electronics*, vol. 54, 2022.
- [38] B. Karki, A. Uniyal, A. Pal, and V. Srivastava, “Advances in surface plasmon resonance-based biosensor technologies for cancer cell detection,” 2022, https://assets.researchsquare.com/files/rs-1480713/v1_covered.pdf?c=1648234334.